Ultrasound monitoring of a deformable tongue-food gel system during uniaxial compression–an in vitro study

Rohit Srivastava, Mathieu Mantelet, Anne Saint-Eve, Jean-Luc Gennisson, Frederic Restagno, Isabelle Souchon, Vincent Mathieu

Ultrasound monitoring of a deformable tongue-food gel system during uniaxial compression–an *in vitro* study

Rohit SRIVASTAVA[a], Mathieu MANTELET[a], Anne SAINT-EVE[a], Jean-Luc GENNISSON[b], Frédéric RESTAGNO[c], Isabelle SOUCHON[d], Vincent MATHIEU[a]

[a]Université Paris-Saclay, INRAE, AgroParisTech, UMR SayFood,

F-78850, Thiverval-Grignon, France

[b]Université Paris-Saclay, CEA, CNRS, Inserm, BioMaps, Service Hospitalier Frédéric Joliot, 91401 Orsay, France

[c]Université Paris-Saclay, CNRS, Laboratoire de physique des solides, 91400 Orsay, France

[d]UMR 408 SQPOV, INRAE, Avignon Université, F-84000 Avignon, France

Declarations of interest: none

Corresponding author:

Vincent Mathieu

Paris-Saclay Food and Bio-product Engineering Laboratory (SayFood UMR 782)

Joint Research Unit INRAE AgroParisTech

Bâtiment CBAI

1, avenue Lucien Brétignières

78850 Thiverval-Grignon, France

Email: vincent.mathieu@inrae.fr

Phone: +33(0)1 30 81 68 13

Fax: +33(0)1 30 81 55 97

Abstract

This study presents a novel ultrasound method for exploring the mechanical deformability of artificial tongue models (ATMs) topped with agar and/or gelatin food gels during uniaxial compression. The ATMs were made from polyvinyl alcohol and displayed different levels of rigidity and surface roughness. We quantified deformation of the ATM-food system as it underwent compression induced by a texture analyzer. We collected real-time measurements via an ultrasound transducer (1 MHz) placed beneath the ATM, enabling to monitor non-invasively the ultrasound time of flight (ToF) and the apparent reflection coefficient (R*) of the ATM-food interface. The results on ToF reflected the tie between the level of force and ATM deformation; they were also precise enough to identify gel fracture. R* was a crucial parameter influenced by both ATM properties (rigidity, surface roughness) and food gel properties (syneresis, ability to mold to surface asperities).

Keywords

Food texture, Oral processing, Ultrasound, Artificial tongue models, Biomimetic set-up

1. Introduction

Food texture perception is the result of complex and dynamic phenomena, which occur simultaneously during food oral processing. Understanding the dynamics of texture perception is hence of paramount interest for food scientists who seek to understand and model consumers' sensorial experience of food (Renard, Van De Velde, & Visschers, 2006; Wilkinson, Dijksterhuis, & Minekus, 2000). As technological advances are made, new and more precise techniques for characterizing food properties (e.g., structure, rheology, and tribology) have been developed (Stokes, Boehm, & Baier, 2013). However, it remains difficult to precisely associate mechanical measurements with sensory attribute ratings and to follow texture dynamics during oral processing. The human oral cavity is very complex and equipped with different types of mechanoreceptors, which can detect both static and dynamic stimuli. The tongue is a crucial organ within the oral cavity: it moves food back and forth, facilitating proper mastication and the safe swallowing of boli. It also plays a very important role in texture perception, especially when food is compressed between the tongue and the palate (Ishihara et al., 2013; Kohyama, Ishihara, Nakauma, & Funami, 2021). During oral processing, the deformation of food over the tongue surface creates clusters of different stimuli, which are perceived by the mechanoreceptors and then sent to the brain for further processing, including texture determination. There is a growing body of literature that underscores how understanding the tongue's physiological properties can shed light on changes in food structure during oral processing and the resulting diversity of texture perceptions (Engelen & Van Der Bilt, 2008; Ketel, de Wijk, de Graaf, & Stieger, 2020; Van Vliet & Primo-Martín, 2011). Therefore, it is essential to further explore the dynamic interactions taking place between food and oral surfaces.

To effectively monitor such interactions, it is necessary to use a non-destructive technique that can be applied in real time. Ultrasound-based approaches have shown great promise and have been successfully employed to visualize tongue movement and bolus swallowing (Gao et al., 2013; Peng, Miethke, Pong, & Lin, 2007). Nevertheless, ultrasound images only provide qualitative information. Therefore, there has been a need to develop ultrasound-based methods with quantitative metrics

78   that can more precisely reveal the occurrence of events at the tongue-food interface. However,

79   quantifying the propagation of ultrasound waves in the human oral cavity can be quite difficult.

80   There is thus a need to develop an oral biomimetic set-up where the behavior of ultrasound waves

81   can be studied in a controlled manner. Mantelet, Restagno, Souchon, & Mathieu (2020) and

82   Mantelet, Srivastava, Restagno, Souchon, & Mathieu (2020) developed a novel ultrasound method

83   for analyzing the tongue-food interface *in vitro*; their research performed a detailed examination of

84   ultrasound reflectivity at the tongue-food interface, characterizing the effects of food properties,

85   lubrication, and tongue surface roughness. This proof-of-concept work utilized rough but non-

86   deformable tongue-mimicking surfaces made of polyvinyl chloride (PVC). It was found that the

87   reflectivity of ultrasound waves (as estimated via the apparent reflection coefficient, R*) at the

88   tongue mimic-food interface could be exploited to monitor changes in contact over time. This

89   research also clarified the influence of food properties and lubrication on R* and, thus, on interface

90   interactions.

91   However, the PVC tongue-mimicking surfaces did not very realistically recreate an actual human

92   tongue, and there was thus further room for improvement. Therefore, in this present article we have

93   introduced a novel artificial tongue-mimicking model (referred to as an ATM hereafter) made of

94   polyvinyl alcohol (PVA). In recent years, PVA has been used in biomedical engineering to model

95   arteries and oral mucosa (Chatelin et al., 2014; Fromageau et al., 2007; Gennisson et al., 2007; Jiang,

96   Liu, & Feng, 2011; Mamada, Fridrici, Kosukegawa, Kapsa, & Ohta, 2011). Tongue mimics made with

97   PVA were also used in our previous study dealing with oral tribology (Srivastava et al., 2021). PVA is a

98   water-soluble synthetic polymer and can be used to form hydrogels. The rigidity of PVA hydrogels

99   can be controlled by varying the number and kinetics of the freezing and thawing cycles (Fromageau

100   et al., 2007). This ability to control hydrogel rigidity made PVA a good fit for our study system.

101   The deformability of the PVA based ATM meant that it could be used in compression experiments in

102   which changes in tongue thickness over time were quantified using an ultrasound parameter called

103 time of flight (ToF). The data gathered helped reveal the relationships among tongue dynamics, food

104 properties, and system deformation. Using the PVA based ATM, we also studied variability in R* in

105 response to ATM properties (i.e., surface roughness, Young's modulus values, and water-release

106 capacity) and food gel properties (i.e., Young's modulus values and water-release capacity), as such

107 factors influence the tongue-food interface and, in turn, affect interactions between food and the

108 tongue.

2. Materials and methods

109

2.1. Preparation and characterization of food gels

110

Preparation of the food gels

111

112 Eight different model gels (Table 1) made of agar and/or gelatin were prepared as described in

113 Mantelet et al. (2020a and b). First, a sucrose solution (white sugar [Cristalco, Paris, France] dissolved

114 in water) was prepared via stirring at 20 °C for 30 min. If needed, agar powder (HP700IFG, Kalys,

115 Bernin, France) was incorporated, and the mixture was heated to 100 °C (until agar was completely

116 dissolved) in a flask sealed with aluminum foil to limit any loss of water. After the agar powder was

117 completely dissolved, the mixture was cooled to 60 °C. This temperature was maintained, and gelatin

118 (Bloom 250 PS 8/3, Rousselot, Gent, Belgium) was added (if required); the mixture was continuously

119 stirred for 20 min. Once the gelatin was completely dissolved, the solution was poured into

120 cylindrical molds (30 mm in diameter, 10 mm in height) made of polyethylene and exposed to

121 conditions promoting gelation (20 °C for 15–18 h). The gel was unmolded just before the experiment

122 to prevent any loss of water or shape over time. Table 1 summarizes the mechanical properties of

123 the gels, which were characterized during the aforementioned research.

124

Water-release capacity of the food gels

125 The water-release properties of these food gels were also quantified using a protocol adapted from

126 Sala, Stieger, & van de Velde (2010). Three Whatman^{TM} filter paper disks (110 mm diameter; GE

127 Healthcare Life Sciences, Chicago, USA) were placed on the base plate of a texture analyzer (TA.XT

128 plus, Stable Micro Systems, Surrey, United Kingdom). A given gel was deposited on the disks and

129 subjected to uniaxial compression (20% strain rate, 10 mm/s); there was a 5 s holding period. The

130 maximum strain rate was chosen to avoid gel breakdown. The amount of water released was

131 determined by comparing filter disk mass before and after the compression test. This methodology

132 was somewhat modified in the case of the $Ag_{0.3}$ gel because the latter was very fragile and released

133 water even without being compressed. Therefore, this gel was left on the filter disks for 5 sec and

134 was then removed, without the application of any external stress. The paper was then weighed as in

135 the case of the other gels. The results are presented in Table 1. However, in all future comparisons,

136 we assumed that $Ag_{0.3}$ had highest water-release capacity.

137 **2.2. Preparation and characterization of the artificial tongue models**

138 <u>Preparation of the artificial tongue models</u>

139 First, PVA powder (Sigma Aldrich, Saint-Louis, USA) was dissolved in ultra-pure water (at 10% w/w)

140 under stirring for 2 h at 80 °C. The solution was then cooled until it reached room temperature. The

141 solution was subsequently poured into cylindrical molds (50 mm in diameter, 20 mm in height) that

142 contained abrasive paper at the bottom. The choice of ATM thickness is based on values reported in

143 literature which ranged from 10 mm to 40 mm (Nakamori et al., 2020; Beghini et al., 2017; Ishihara

144 et al., 2013). To simulate two levels of surface roughness, two types of abrasive paper were used: (i)

145 P80 sandpaper (grain size = 200 µm; Struers, Champigny-sur-Marne, France) and (ii) P40 sandpaper

146 (grain size = 425 µm; Norton, Saint-Gobain, France). Hereafter, they are referred to as R_1 and R_2,

147 respectively. The molds were sealed and frozen at -20 °C for 10 h. They were then thawed for 14 h at

148 20 °C. The freezing and thawing cycles were adjusted to attain the desired rigidity (Fromageau et al.,

149 2007). Two types of ATMs were prepared: a soft ATM (C_2), which underwent two cycles, and a hard

150 ATM (C_6), which underwent six cycles. After the completion of the requisite number of cycles, the

6

151   ATMs were unmolded and stored in reverse osmosis treated water at room temperature (20 °C) for

152   several months.

153   <u>Mechanical properties of the artificial tongue models</u>

154   ATM rigidity was measured using uniaxial compression tests carried out with a texture analyzer

155   (speed: 10 mm/s; strain rate: up to 20%; at least 3 replicates performed). This protocol was adapted

156   from the work of Gao, Nakao, Ishihara, Funami, & Kohyama (2016). The resulting Young's modulus

157   values are presented in Table 2.

158   <u>Water-release capacity of the artificial tongue models</u>

159   The ability of the ATMs to release water under mechanical compression was also quantified. For each

160   ATM, any surface water was gently absorbed with Kimtech™ absorbent wipes (Kimberly-Clark, Irving,

161   TX, USA) until the tissue came away dry. Subsequently, three layers of absorbing Whatman™ filter

162   paper (110 mm diameter; GE Healthcare Life Sciences, Chicago, USA) were placed between the

163   texture analyzer probe and the tongue's rough surface to fully collect the water released. We chose

164   to use a strain rate of 5% and a holding time of 5 sec to avoid any damage to the tongue's surface

165   from the aluminum probe. The difference in paper mass was then determined as previously

166   described to estimate water-release capacity (Table 2).

167   <u>Surface roughness profiles of the artificial tongue models</u>

168   ATM surface roughness was analyzed via profilometry. Measurements were obtained using a contact

169   profilometer (Dektak XT, Brucker, Billerica, MA, USA) with a 50-nm-radius stylus and 1 mg of applied

170   force. For each ATM, three 30 mm surface scans were performed (one-dimensional, 45° of rotation

171   between each scan). Vision 64 software (Bruker, Billerica, MA, USA) was used to control, analyze, and

172   perform slope corrections before employing an algorithm in MATLAB (The MathWorks, Natick,

173   Massachussetts, USA) to calculate roughness. Two parameters were chosen: the mean height of

174   surface asperities (Ra) and correlation length, which is inversely related to asperity density (β).

175 Although only two types of sandpaper were used, the freezing and thawing cycles had an impact on

176 surface roughness as well. The values are presented in Table 2.

177 **2.3. Ultrasound measurements**

178 As in Mantelet et al. (2020a and b), the ultrasound set-up (Figure 1) comprised a texture analyzer, a

179 tongue-mimicking surface (a PVA based ATM in this study), and a mono-element piezoelectric

180 ultrasound transducer (central frequency of 1 MHz; V103RM, Olympus, Shinjuku, Tokyo, Japan); the

181 latter was placed beneath the ATM. Before starting each experimental test, the water on the surface

182 of the ATM was gently removed using absorbent wipes (Kimtech^{TM}, Kimberly-Clark, Irving, TX, USA)

183 until the tissue came away dry. The food gels were gently unmolded and placed on top of the ATM.

184 The texture analyzer was used to apply a controlled uniaxial deformation (of up to 8 mm at 10 mm/s)

185 to the ATM-food gel system using a circular aluminum probe (diameter: 40 mm). Ultrasound

186 measurements were made prior to the food being placed on the ATM (i.e., reference measurements)

187 and in real time during the compression period. To this end, the transducer, acting as both an emitter

188 and a receiver (pulse-echo mode), was used in tandem with a pulser-receiver (Sonatronic, Evry,

189 France). The pulser-receiver system was used to generate negative square wave pulses (width: 500

190 ns, amplitude: 80 V) and to digitize the radio frequency (*rf*) signals corresponding to the system's

191 pulse echo response (12-bit quantification, 100 MHz sampling rate, 38 dB gain). The frequency of

192 pulse recurrence was around 90 Hz. A LabVIEW (National Instrument, Austin, Texas, USA) interface

193 was used for real-time acquisition of the *rf* signals during the compression period.

194 **2.4. Signal processing**

195 Similarly to the work done in our previous research Mantelet et al. (2020a and b), the apparent

196 reflection coefficient of ATM-food interface (R*) was calculated on all the ultrasound signals of each

197 test. ATM deformability had an impact on both the amplitude and the time of occurrence of the

198 ultrasound waves reflecting off the ATM-food gel interface. The deformations induced during

199 compression shortened the path to be covered by the waves. As a consequence, the time needed for

200   the waves to travel between the emission source and back was shorter as well. Thus, in addition to

201   R*, here we have used another ultrasound parameter: time of flight (ToF).

202   Each experimental test is composed of a set of signals which have been analyzed using Matlab.

203   Figure 2a shows the typical shape of an *rf* signal, composed of two main echoes: E_0 for the tongue-

204   food interface, E_1 for the food-palate interface. Figure 2b shows the M-Mode representation of the

205   whole set of signals acquired during a test, where signal amplitude is coded in color and thus allows

206   to trace the evolution of the echoes identified in Figure 2a. For each signal, noise reduction was

207   implemented via a low-pass filter (cut-off frequency: 10 MHz). To precisely characterize ATM

208   deformation, it was crucial to accurately determine the ToF for the echo, E_0, associated with the

209   ATM-food gel interface over the entire course of a given test. E_1 echo was not processed for this

210   study. Using the reference signal, a time window was automatically defined; it had a width of 5 μs

211   and was centered with respect to the Hilbert-transformed peak amplitude of the signal. This window

212   of reference was then cross-correlated with all the *rf* signals acquired during a given test, allowing

213   the automatic detection of the ToF associated with E_0.

214   The ToF associated with the echo E_0 corresponds to the time required for the ultrasonic wave to

215   return to the sensor after being reflected at the interface between the ATM and the food. The

216   thickness (e) of the ATM is proportional to this time of flight ToF:

217
$$e = \frac{1}{2} . ToF . c$$

218   Where c is the propagation speed of ultrasound waves in the 10% PVA hydrogels (1540 m/s at 20 °C;

219   Gennisson et al., 2007). Finally, the deformation of the ATM (Δe) was deduced by subtracting the real

220   time thickness (e) of the ATM from its initial value e_0. As an example for validation of the accuracy of

221   the method, we compared it with deformation measurements assessed with the texture analyzer. To

222   do so, we considered the compression of an ATM without any food. The deformation applied was

223   20%, with a velocity equal to 10 mm/s (similarly to as done for the tests in presence of food). Three

224 repetitions were performed. The obtained average curves with standard deviation envelopes can be

225 compared in Figure 3. The obtained graphs hence show that the deformation measurements by both

226 ultrasound and texture analyzer are in agreement, confirming the relevance of the ultrasound

227 velocity value (1540 m/s) used for the calculation, and validating the method for tongue deformation

228 assessment.

229 To reliably calculate R* at the ATM-food gel interface, it was necessary to accurately estimate the

230 amplitude of E_0. For all the *rf* signals, time windows encompassing E_0 had a width of 5 μs and were

231 defined so as to be centered around the ToF for E_0. A Hanning window was applied, and the

232 amplitude of E_0 was defined as the maximum amplitude of the power spectrum (the Fourier

233 transform of the autocorrelation function) for the window obtained. R* was defined as E_0's

234 amplitude during a given test, expressed as a percentage of E_0's amplitude during the reference

235 measurements (i.e., when there was no food gel on the ATM). Consequently, the evolution of ToF

236 and R* were computed for the entire duration of an experimental test, as illustrated in Figure 2c

237 which focuses on the compression step.

3. Results and discussion

238

239 To begin with, the biomimetic set-up with different ATMs was developed. The roughness and rigidity

240 values (Table 2) of the ATMs fabricated for this study were found to be in accordance with the values

241 reported for real human tongues. Ishihara et al., (2013) has reported the rigidity of the human

242 tongue at rest as 12.2 ± 4.2 kPa and at contracted state as 122.5 ± 58.5 kPa. Moreover, the surface

243 asperities height (filiform papillae) of human tongue was reported between 50 - 150 μm (Andablo-

244 Reyes et al., 2020; Wang, Wang, Upadhyay, & Chen, 2019). Also, Andablo-Reyes et al. (2020)

245 reported average diameter of filiform papillae around 350 μm. Hence the characteristics of the

246 developed ATMs were in good accordance with the values published in literature on human tongues.

247 The results and discussion on these ATMs are discussed below and have been structured into two

248 main parts that each focus on one of ultrasound parameters: (i) ToF and (ii) R*.

3.1. Characterizing the deformation of the artificial tongue models—ToF

It is important to investigate the deformation of the tongue during oral processing because this phenomenon can directly change food bolus characteristics and stimulate the mechanoreceptors responsible for texture perception. In this study, our *in vitro* approach allowed us to measure the ToF of the ultrasound waves reflected off of the ATM-food gel interface, providing an accurate estimate of ATM deformation during the uniaxial compression of the system. The maximum possible degree of ATM deformation (in the absence of food) was 40% because initial ATM thickness was 20 mm, and the level of deformation applied to the system was fixed at 8 mm. It is also important to have in mind that the diameter of the ultrasound beam (less than 10 mm) is lower than the diameter of the gels. Thus, the deformations measured by ultrasound only reflect what is happening in the central part of the ATM, which can be assumed as planar.

Effect of food properties

When the soft (C_2R_2) ATM was used, varied profiles of force (as measured by the texture analyzer) were observed over the range of food gels (plate displacement: 8 mm at 10 mm/s; Figure 4a). The ToF values obtained during these experimental tests showed that ATM deformation changed over time (Figure 4b). Force and ATM deformation showed similar trends. When tests were performed using the hard (C_6R_2) ATM, we saw the same patterns and similarity in metric values (Figures 4c and 4d). These results are encouraging because they underscore the relationship between ATM deformation and the force applied to the system during compression. The *in situ* and non-invasive characterization made possible here with ultrasound gives promising long term *in vivo* perspectives. Forces and deformations indeed constitute very relevant information to monitor during oral processing, but they remain impossible to characterize so far. The ToF values also showed that it was possible to identify the fracture point of food gels during compression. Like the level of force, tongue deformation was found to be sensitive to the sudden breakage of food gels. Out of the eight food

273 gels, $Ag_{0.3}$ was the only one that fractured during compression, and this event was easily observed in

274 both the ATM deformation results and the force results.

275 It is also clear from the results that ATM deformation was affected by the mechanical properties of

276 the food gels. For example, because $Ag_{0.3}$ and $Ge_{3.5}$ were softer, they did not cause as much ATM

277 deformation as did the more rigid food gels like $Ag_{1.8}$. To understand this phenomenon, it is useful to

278 make the comparison with the situation of two springs connected in series. Total deformation is the

279 sum of the strains experienced by the individual springs. Hence, the softer gels more equally shared

280 the deformation resulting from system compression, whereas the more rigid gels did not, leading the

281 ATM to deform more in compensation.

282   Effect of artificial tongue model properties

283 The human tongue is a complex muscular organ that is also a hydrostat. In other words, its volume

284 remains constant when its rigidity is modulated or when it is in motion (Napadow, Chen, Wedeen, &

285 Gilbert, 1999). Tongue rigidity changes considerably over the course of oral processing to better

286 manage the bolus and texture perception. We used the PVA based ATM to investigate the role of

287 rigidity in food deformation. We measured force and ATM deformation during experimental tests in

288 which the different food gels were placed on the soft and hard ATMs (C_2R_2 and C_6R_2, respectively;

289 values following compression: Figure 5). ATM rigidity affected the relationship between the level of

290 force and ATM deformation. For both ATM types, the different food gels formed clusters that were

291 based on the gels' mechanical properties). It represents that the diversity in mechanical property of

292 gels were suitable for this study. Some food gels, like $Ag_{0.3}$, resulted in little tongue deformation,

293 while others, like $Ag_{1.8}$, led to nearly 8 mm in deformation in the soft ATM, suggesting that the food

294 gels themselves were not deformed at all. Taken together, the clusters of points for each ATM type

295 followed a specific pattern, which was comparable to the curves obtained for the Young's modulus

296 values during ATM compression. It is thus evident that the hard ATM led to greater force than did the

297 soft ATM. Moreover, ATM rigidity also influenced food deformation kinetics. Using $Ag_{0.3}$ as an

298 example, both the force and ATM deformation results show that gel fracture occurred earlier on the

299 hard ATM than on the soft ATM (Figure 4). These results highlight that ATM rigidity plays an

300 important part in shaping the extent and kinetics of food deformation.

301 The human tongue has a particular surface topology due to the presence of different papillae.

302 However, the latter's role in the bulk deformation of food has yet to be thoroughly explored. In this

303 study, force and ATM deformation displayed different patterns over time when certain food gels

304 (notably gelatin-dominant gels) were placed on ATMs with the same rigidity but different surface

305 roughness. For example, in case of the gelatin-dominant gels $Ge_{3.5}$ and Ge_7, the effect of surface

306 roughness on tongue deformation was much more pronounced for the hard ATM (Figures 6a, b),

307 since the deformation curve for C_6R_1 was more distant from C_6R_2 when comparing C_2R_1 with C_2R_2. The

308 explanation could be that, when the cylindrical gels were compressed on top of the ATM, a barreling

309 effect arose from friction and adhesion coming into play (Brennan & Bourne, 1994; Pons & Fiszman,

310 1996). Barreling effects occur when there is friction between a plate and a specimen, which results in

311 a state of triaxial stress instead of the ideal state of uniaxial stress. Since gelatin polymers have

312 adhesive properties and release less water, the degree of friction might have been greater. The agar-

313 dominant gels did not display such a pattern, perhaps because of their higher degree of water

314 release.

315 This explanation could also apply to the results for the hard ATM, which released less water during

316 compression. Furthermore, the number of freezing and thawing cycles positively affected mean peak

317 asperity height (Table 2). The presence of taller asperities with negligible water in the interphase

318 region should have enhanced adhesion between the food gels and the ATM. Greater adhesion can

319 enhance barreling effects, lowering the uniaxial force exerted on the system.

320   **3.2. Analysis of the tongue model-food gel interface—R***

321 R* is the parameter used to quantify the apparent reflection of ultrasound waves at the interface

322 between the ATM and the food gels, and its value is greatly dependent on the media's difference in

13

acoustic impedance (Mantelet et al., 2019). R* has been shown to be a key parameter for understanding the characteristics of the tongue-food interface (Mantelet et al., 2020a and b). More specifically, it was found that there was a pronounced difference in acoustic impedance between a PVC tongue-mimicking surface and various food gels, resulting in the strong reflection of ultrasound waves at the interface. Here, in contrast, the PVA based ATM and the food gels appeared to have similar acoustical impedance, PVA being thus more representative of the acoustic properties of human soft tissue. However, it may also mean that the quantity of acoustic energy reflected by the ATM-food gel interface was limited. That said, there were clear differences in R* among food gels (Figure 7a). Results for the C_2R_2 ATM underscore the sensitivity of our ultrasound method when it comes to analyzing the interface between the PVA ATM (with its more biologically realistic properties) and the food gels. Previous research has examined variation in R* for a PVC tongue-mimicking surface (Mantelet et al., 2020a and b). The presence of trapped air at the interface was found to be a key factor affecting R* variations. The value of this parameter was at a minimum when no air was present, representing a state of perfect coupling between the ATM and food gel; in contrast, when R* was maximum, coupling was imperfect due to significant amounts of trapped air. Factors that can alter air presence are water release or mechanical deformation. The results obtained here were similar to those seen in the previous study. R* values varied depending on food gel type and the amount of water present at the interface.

Effect of food gel properties

Polymers like agar or gelatin form very different structures upon gelation, resulting in products that differ in rigidity and water-release capacity (Santagiuliana, Piqueras-Fiszman, van der Linden, Stieger, & Scholten, 2018). Consequently, we observed a variety of changes in R* over time: it decreased, plateaued, or increased over the course of compression, indicating the presence of a nonlinear response. It was therefore necessary to study the data quantitatively. When the values of R* were examined and compared for two time points (Figure 7b), t_0 (test begins—food gel is deposited on the

14

348   ATM) and t_1 (test ends following the compression period), it was evident that two main factors were

349   at play. Syneresis and the gel's ability to mold itself to ATM surface asperities appeared to govern

350   changes in R* over time.

351   At t_0 (Figure 7b), the R* value for $Ag_{0.3}$ was quite low since the latter was an extremely soft food gel

352   that released a large amount of water, improving contact with the ATM's surface. $Ge_{3.5}$ had a

353   comparatively higher R* value despite its nearly equivalent Young's modulus value because it

354   released less water. The values at t_0 can shed some light on why some food gels might be perceived

355   as dry or wet when deposited on the tongue.

356   When the food gels were compressed on the ATM, the main trend observed was a decrease of R*

357   since the application of stress tended to improve contact at the interface. The R* values following

358   compression (t_1) provided much needed insight into the role of food gel and ATM properties in

359   predicting the degree of improvement in contact. The higher the gel's gelatin concentration, the

360   higher the initial R* value, suggesting poorer levels of contact. There was thus greater room for

361   improvement when the uniaxial stress was applied. This difference was starker for the more rigid

362   gelatin-dominant gels since the force exerted to achieve 8 mm in deformation was much higher,

363   resulting in better contact between the food gel and the ATM.

364   Effect of artificial tongue model properties

365   ATM properties also influenced the R* values. When examining how ATM rigidity type (C_2R_2 = soft

366   and C_6R_2 = hard) affected the results obtained with the food gels $Ag_{0.3}$, $Ge_{3.5}$, Ge_7, and Ge_{7T}, it was

367   found that R* was higher at the start of the tests (t_0) for C_6R_2 compared to C_2R_2 (Figures 8a and 8b).

368   The greater the number of freezing-thawing cycles, the denser and more rigid the PVA becomes,

369   affecting the polymer's ability to release water. The resulting absence of water at the interface could

370   explain why R* was higher for the C_6R_2 ATM. As discussed previously, low levels of lubrication at the

371   interface can augment adhesion, resulting in a barreling effect and an uneven decline in compression

372   force. This barreling effect might lead to uneven surface deformation as well as air pockets, thus

15

373   increasing R*. Another explanation could be that the hard ATM underwent six cycles of freezing and

374   thawing, more greatly affecting its surface roughness (peak height) even though sandpaper grain size

375   was the same. Increased asperity height could have led to more air being trapped at the interface,

376   boosting R* values.

377   When rigidity was controlled, ATM surface roughness (C_2R_1 vs. C_2R_2) was found to affect R* values

378   (Figures 9a and 9b): it resulted in different temporal patterns in R* for the three gelatin-dominant

379   gels ($Ge_{3.5}$, Ge_7, Ge_{7T}). R* values were higher for C_2R_1 than for C_2R_2, which was an unexpected result

380   because one would assume that higher asperities would lead to more trapped air, enhancing wave

381   reflection. However, it should also be noted that, compared to C_2R_1, C_2R_2 had a larger peak

382   correlation length (β) (i.e., wider peaks) and hence a lower peak density. Peak density could affect

383   surface topography overall, potentially explaining this unexpected observation.

384   The comparison of the R* values for Ge_7 versus Ge_{7T} sheds light on the ability of TWEEN to modify

385   interface characteristics (Figure 9c). As a surfactant, TWEEN lowers the surface tension of water,

386   promoting its spread under conditions of compression and expelling the air trapped among

387   asperities. It seems likely that the properties of the surfactant in Ge_{7T} reduced the difference in the

388   R* values when this food gel was used on ATMs of different surface roughness.

389   ## 4. Conclusions

390   In this study, we used PVA based ATMs with different bulk rigidities and surface roughness profiles to

391   investigate the role of tongue deformability in the mechanical compression of food gels by a hard

392   palate. The ToF of the ultrasound wave traveling to and from the ATM-food gel interface was used as

393   a key metric for characterizing the overall deformation of the system. The ToF values helped

394   estimate ATM deformation during the uniaxial compression of the food gels and were found to fit

395   with the force exerted on the system. R*, or the apparent reflection coefficient, has been employed

396   in previous studies to analyze tongue-food dynamics. It was found to be effective here as well for

397 characterizing real-time changes at the ATM-food gel interface over the course of compression,

398 including changes in the relationship between contact dynamics and both gel properties (i.e., Young's

399 modulus values, water-release capacity) and ATM properties (i.e., deformability and surface

400 roughness). More importantly, this study demonstrated that, despite the similarities in the acoustical

401 impedance of the ATMs and the food gels, it was possible to accurately quantify reflection at a rather

402 small scale. Consequently, this approach may hold promise for *in vivo* applications involving

403 biological tissues and food, which have similar acoustical properties.

404 The study also underscored the utility of PVA in ATM design, given that it is a material that can better

405 replicate tongue rigidity and roughness, a need that still exists in food oral processing research.

406 Additionally, our findings showed that ultrasound techniques could be useful for tracking

407 quantitative information related to mechanical interactions between the tongue and the palate.

408 Future work using this set-up will focus on investigating how ultrasound indicators respond when

409 investigating systems with more complex, heterogeneous model foods. The broader goal is to

410 progressively bridge the gap between model food and real food. Future research will also better

411 account for the complexity of food oral processing, a greater diversity of motion (mixing shearing and

412 compression) will be simulated and tongue shape, oral cavity anatomy and oral temperature will be

413 more realistically recreated to further put ultrasound techniques to the test, prior to their more

414 widespread use *in vivo*.

Acknowledgments

References

Beghini, M., Pereira, T. L., Montes, J. M. C., De Moura, D. V., Dezem, T. U., …. De Lima Pereira, S. V. (2017). Morphometric Analysis of Tongue in Individuals of European and African Ancestry. *Journal of Forensic Investigation*, *5*(1). https://doi.org/10.13188/2330-0396.1000038

Andablo-Reyes, E., Bryant, M., Neville, A., Hyde, P., Sarkar, R., Francis, M., & Sarkar, A. (2020). 3D Biomimetic Tongue-Emulating Surfaces for Tribological Applications. *ACS Applied Materials and Interfaces*, *12*(44), 49371–49385. https://doi.org/10.1021/acsami.0c12925

BRENNAN, J. G., & BOURNE, M. C. (1994). Effect of Lubrication on the Compression Behaviour of Cheese and Frankfurters. *Journal of Texture Studies*, *25*(2), 139–150. https://doi.org/10.1111/j.1745-4603.1994.tb01322.x

Chatelin, S., Bernal, M., Deffieux, T., Papadacci, C., Flaud, P., Nahas, A., … Pernot, M. (2014). Anisotropic polyvinyl alcohol hydrogel phantom for shear wave elastography in fibrous biological soft tissue: A multimodality characterization. *Physics in Medicine and Biology*, *59*(22), 6923–6940. https://doi.org/10.1088/0031-9155/59/22/6923

Engelen, L., & Van Der Bilt, A. (2008). Oral physiology and texture perception of semisolids. *Journal of Texture Studies*, *39*(1), 83–113. https://doi.org/10.1111/j.1745-4603.2007.00132.x

Fromageau, J., Gennisson, J. L., Schmitt, C., Maurice, R. L., Mongrain, R., & Cloutier, G. (2007). Estimation of polyvinyl alcohol cryogel mechanical properties with four ultrasound elastography

methods and comparison with gold standard testings. *IEEE Transactions on Ultrasonics, Ferroelectrics, and Frequency Control*, *54*(3), 498–508. https://doi.org/10.1109/TUFFC.2007.273

Gao, Z., Nakao, S., Ishihara, S., Funami, T., & Kohyama, K. (2016). A Pilot Study on Ultrasound Elastography for Evaluation of Mechanical Characteristics and Oral Strategy of Gels. *Journal of Texture Studies*, *47*(2), 152–160. https://doi.org/10.1111/jtxs.12170

Gennisson, J.-L., Rénier, M., Catheline, S., Barrière, C., Bercoff, J., Tanter, M., & Fink, M. (2007). Acoustoelasticity in soft solids: Assessment of the nonlinear shear modulus with the acoustic radiation force. *The Journal of the Acoustical Society of America*, *122*(6), 3211–3219. https://doi.org/10.1121/1.2793605

Ishihara, S., Nakao, S., Nakauma, M., Funami, T., Hori, K., Ono, T., … Nishinari, K. (2013). Compression Test of Food Gels on Artificial Tongue and Its Comparison with Human Test. *Journal of Texture Studies*, *44*(2), 104–114. https://doi.org/10.1111/jtxs.12002

Jiang, S., Liu, S., & Feng, W. (2011). PVA hydrogel properties for biomedical application. *Journal of the Mechanical Behavior of Biomedical Materials*, *4*(7), 1228–1233. https://doi.org/10.1016/j.jmbbm.2011.04.005

Ketel, E. C., de Wijk, R. A., de Graaf, C., & Stieger, M. (2020). Relating oral physiology and anatomy of consumers varying in age, gender and ethnicity to food oral processing behavior. *Physiology and Behavior*, *215*(August 2019), 112766. https://doi.org/10.1016/j.physbeh.2019.112766

Kohyama, K., Ishihara, S., Nakauma, M., & Funami, T. (2021). Fracture phenomena of soft gellan gum gels during compression with artificial tongues. *Food Hydrocolloids*, *112*(August 2020), 106283. https://doi.org/10.1016/j.foodhyd.2020.106283

Mamada, K., Fridrici, V., Kosukegawa, H., Kapsa, P., & Ohta, M. (2011). Friction properties of poly(vinyl alcohol) hydrogel: Effects of degree of polymerization and saponification value. *Tribology Letters*, *42*(2), 241–251. https://doi.org/10.1007/s11249-011-9768-8

466 Mantelet, M., Panouillé, M., Boué, F., Bosc, V., Restagno, F., Souchon, I., & Mathieu, V. (2019).

467 Impact of sol-gel transition on the ultrasonic properties of complex model foods: Application to

468 agar/gelatin gels and emulsion filled gels. *Food Hydrocolloids*, *87*(May 2018), 506–518.

469 https://doi.org/10.1016/j.foodhyd.2018.08.021

470 Mantelet, M., Restagno, F., Souchon, I., & Mathieu, V. (2020). Using ultrasound to characterize the

471 tongue-food interface: An in vitro study examining the impact of surface roughness and

472 lubrication. *Ultrasonics*, *103*(April 2019), 106095. https://doi.org/10.1016/j.ultras.2020.106095

473 Mantelet, M., Srivastava, R., Restagno, F., Souchon, I., & Mathieu, V. (2020). Real time ultrasound

474 assessment of contact progress between food gels and tongue mimicking surfaces during a

475 compression. *Food Hydrocolloids*, 106099. https://doi.org/10.1016/j.foodhyd.2020.106099

476 Nakamori, M., Imamura, E., Fukuta, M., Tachiyama, K., Kamimura, T., Hayashi, Y., … Wakabayashi, S.

477 (2020). Tongue thickness measured by ultrasonography is associated with tongue pressure in

478 the Japanese elderly. *PLoS ONE*, *15*(8 July), 1–12.

479 https://doi.org/10.1371/journal.pone.0230224

480 Napadow, V. J., Chen, Q., Wedeen, V. J., & Gilbert, R. J. (1999). Intramural mechanics of the human

481 tongue in association with physiological deformations. *Journal of Biomechanics*, *32*(1), 1–12.

482 https://doi.org/10.1016/S0021-9290(98)00109-2

483 Pons, M., & Fiszman, S. M. (1996). Instrumental texture profile analysis with particular reference to

484 gelled systems. *Journal of Texture Studies*, *27*(6), 597–624. https://doi.org/10.1111/j.1745-

485 4603.1996.tb00996.x

486 Renard, D., Van De Velde, F., & Visschers, R. W. (2006). The gap between food gel structure, texture

487 and perception. *Food Hydrocolloids*, *20*(4), 423–431.

488 https://doi.org/10.1016/j.foodhyd.2005.10.014

489 Sala, G., Stieger, M., & van de Velde, F. (2010). Serum release boosts sweetness intensity in gels.

490   *Food Hydrocolloids*, *24*(5), 494–501. https://doi.org/10.1016/j.foodhyd.2009.12.001

491   Santagiuliana, M., Piqueras-Fiszman, B., van der Linden, E., Stieger, M., & Scholten, E. (2018).

492   Mechanical properties affect detectability of perceived texture contrast in heterogeneous food

493   gels. *Food Hydrocolloids*, *80*, 254–263. https://doi.org/10.1016/j.foodhyd.2018.02.022

494   Srivastava, R., Bosc, V., Restagno, F., Tournier, C., Menut, P., Souchon, I., & Mathieu, V. (2021). A new

495   biomimetic set-up to understand the role of the kinematic, mechanical, and surface

496   characteristics of the tongue in food oral tribological studies. *Food Hydrocolloids*, *115*(July

497   2020). https://doi.org/10.1016/j.foodhyd.2021.106602

498   Stokes, J. R., Boehm, M. W., & Baier, S. K. (2013). Oral processing, texture and mouthfeel: From

499   rheology to tribology and beyond. *Current Opinion in Colloid and Interface Science*, *18*(4), 349–

500   359. https://doi.org/10.1016/j.cocis.2013.04.010

501   Van Vliet, T., & Primo-Martín, C. (2011). Interplay Between Product Characteristics, Oral Physiology

502   And Texture Perception Of Cellular Brittle Foods. *Journal of Texture Studies*, *42*(2), 82–94.

503   https://doi.org/10.1111/j.1745-4603.2010.00273.x

504   Wang, X., Wang, X., Upadhyay, R., & Chen, J. (2019). Topographic study of human tongue in relation

505   to   oral   tribology.   *Food   Hydrocolloids*,   *95*(April),   116–121.

506   https://doi.org/10.1016/j.foodhyd.2019.04.022

507   Wilkinson, C., Dijksterhuis, G. B., & Minekus, M. (2000). From food structure to texture. *Trends in

508   Food Science and Technology*, *11*(12), 442–450. https://doi.org/10.1016/S0924-2244(01)00033-

509   4

510

511

512

513

514

Figure Captions

Figure 1: (a) Schematic representation of the experimental set-up; Pictures of (b) the polyvinyl alcohol artificial tongue model (ATM) and (c) the ATM topped with a food gel.

Figure 2: (a) A typical *rf* signal, composed of two main echoes: E_0 for the tongue-food interface, E_1 for the food-palate interface; (b) Ultrasound M-mode imaging of the entire set of signals obtained during an experiment and (c) Variation of ToF and R* (calculated on the basis of E_0) during a compression.

Figure 3: Estimation of the tongue deformation (without food) by ultrasound time of flight and texture analyzer.

Figure 4: (a) Force and (b) estimated ATM deformation over time as food gels were compressed on the soft ATM (C_2R_2); (c) Force and (d) estimated ATM deformation over time as food gels were compressed on the hard ATM (C_6R_2). The cloud around each line represents the standard deviation; at least six replicates were performed for each experimental test. The markers of different shapes were used to enhance the readability of the graphs. The dotted line on ATM deformation plot represents the maximum deformation imposed by the texture analyzer.

Figure 5: Force and estimated ATM deformation following compression (time t_1) for the experimental tests conducted with all the food gel types on ATMs differing in rigidity (C_2R_2 = soft and C_6R_2 = hard). Each color corresponds to a certain food gel type, whereas the two symbols distinguish between the ATM types.

Figure 6: Effect of surface roughness on estimated ATM deformation during the compression of the food gels (a) $Ge_{3.5}$ and (b) Ge_7. The cloud around each line represents the standard deviation.

535 <u>Figure 7</u>: (a) R* values during the compression of the food gels on the soft ATM (C_2R_2); the cloud

536 around each line represents the standard deviation; the markers of different shapes were used to

537 enhance the readability of the graphs. (b) R* values before compression began (t_0), and after

538 compression ended (t_1), and the difference between the two (t_0-t_1). The error bars represent the

539 standard deviations.

540 <u>Figure 8</u>: Effect of ATM rigidity on R* during the compression of the food gels on (a) the soft ATM

541 (C_2R_2) and (b) the hard ATM (C_6R_2). The error bars represent the standard deviations.

542 <u>Figure 9</u>: Effect of surface roughness on R* during the compression of the food gels (a) $Ge_{3.5}$, (b) Ge_7,

543 and (c) Ge_{7T}. The cloud around each line represents the standard deviation.

544

545

546

547

548

549

550

551

552

553

554

555

556

557

558

Tables

Table 1: Description of the food gels (Diameter: 30 mm; Height: 10 mm): composition (they all contained 15% wt of sucrose), Young's modulus values, and water-release capacity. Standard deviations are provided when applicable.

Table 2: Description of the ATMs (Diameter: 50 mm; Height: 20 mm): Young's modulus values, surface roughness profiles, and water-release capacity. Standard deviations are provided when applicable.

566

567

568

569

570

571

572

573

574

575

576

577

581 Figure 1

582

583

Figure 2

601
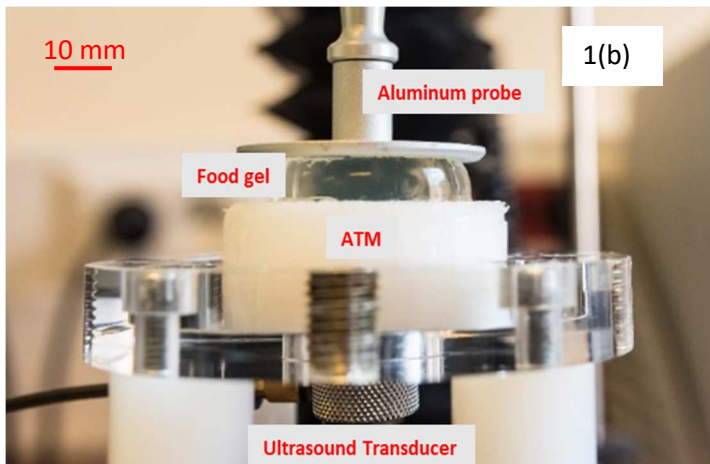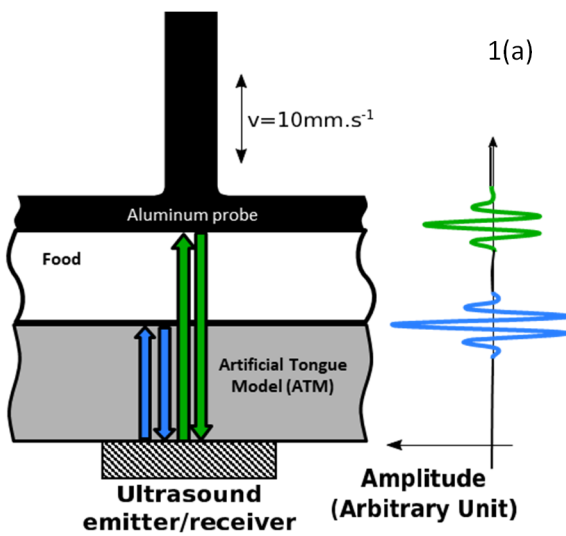
602

603

604

605

606

607

608

609

610

611

612

613

614

615

616

617

2(a) **Ultrasound signal**

E_0 (tongue/food)

E_1 (food/palate)

2(b) **Ultrasound M-mode image**

E_0

E_1

Compression   Relaxation

2(c) **US indicators from echo E_0**

618

619

620
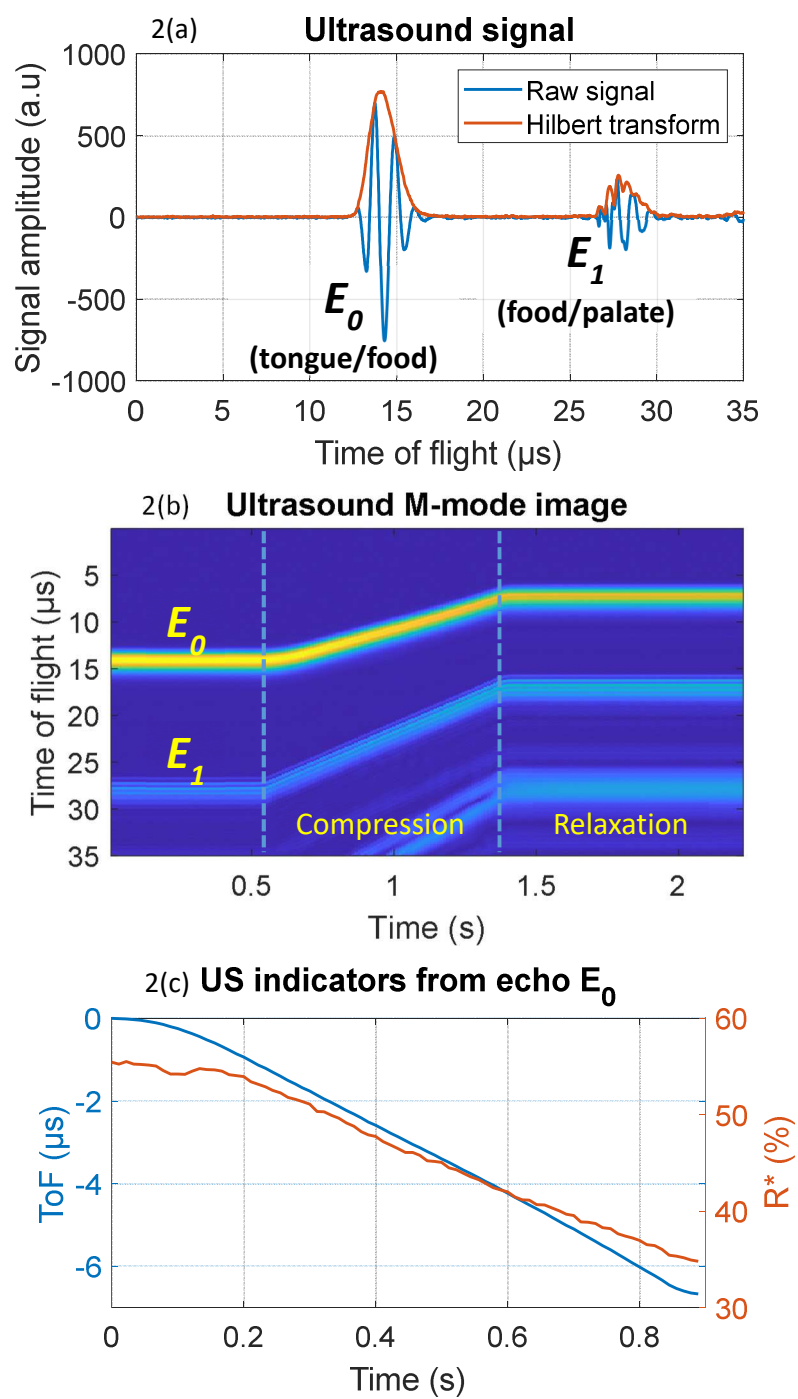
Figure 3

622

623

624

625

626

627

628

629

630

631

632

633

634

635

636

637
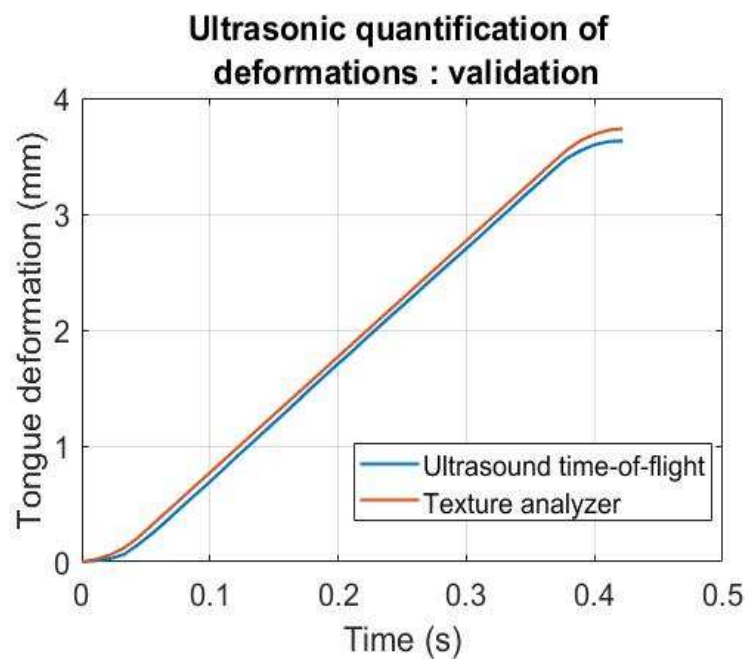
638

639

640
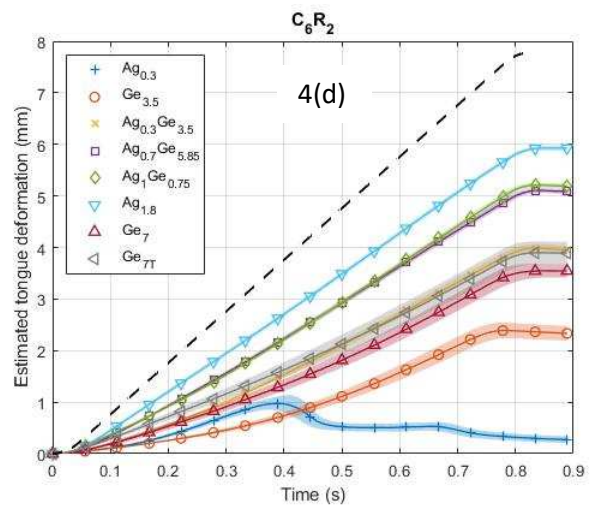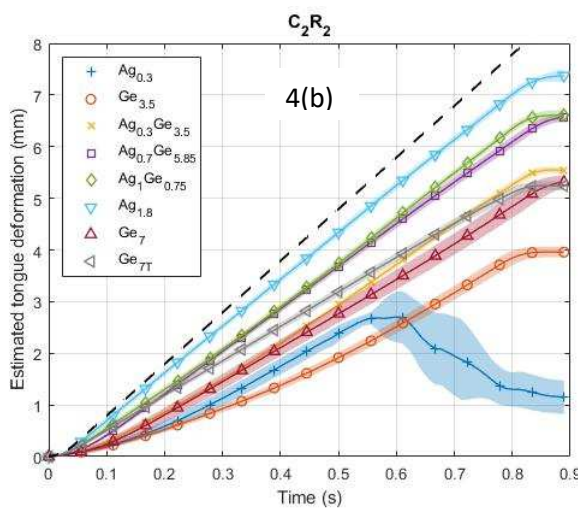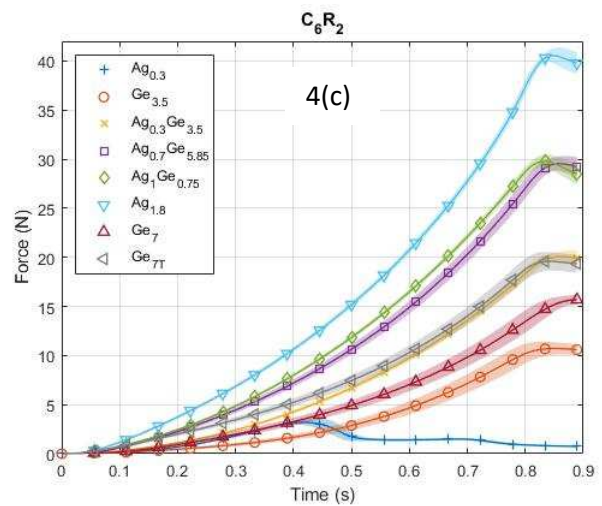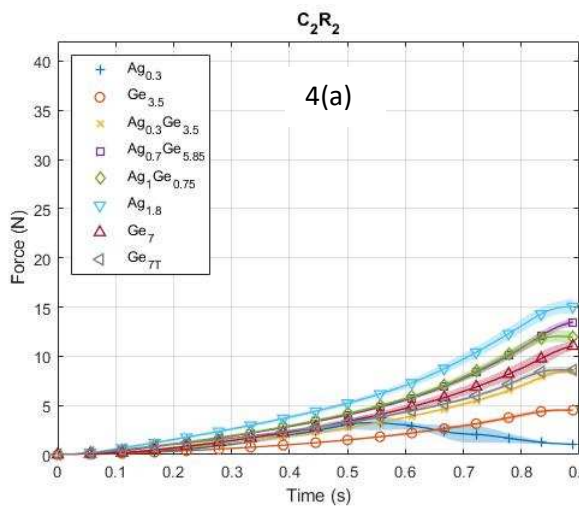
Figure 4

653

654

655

656

657
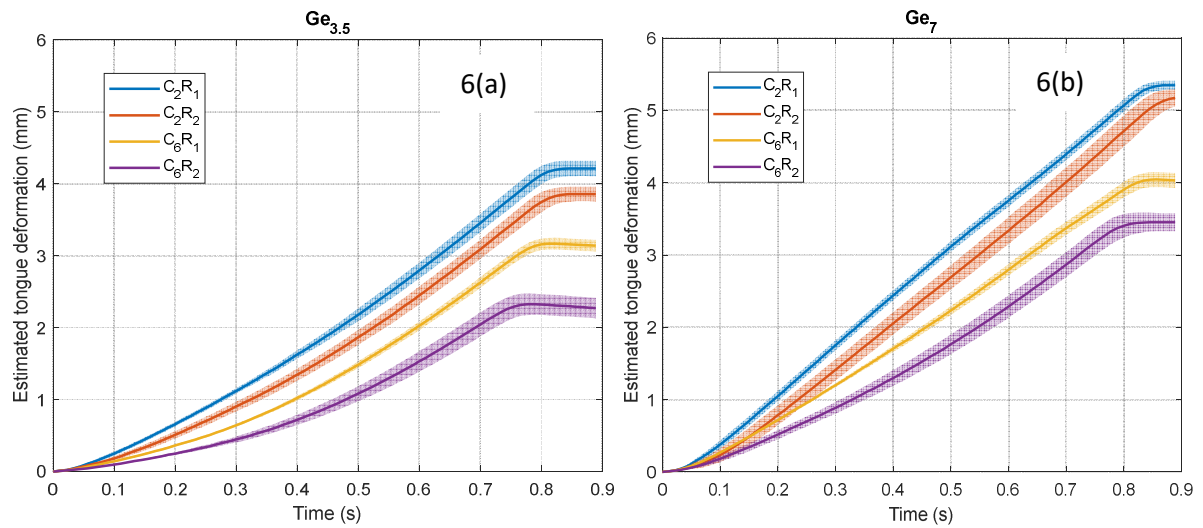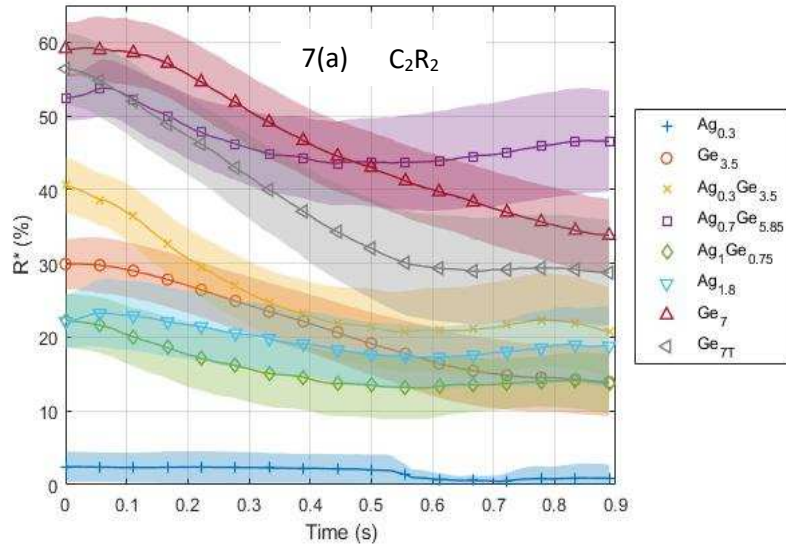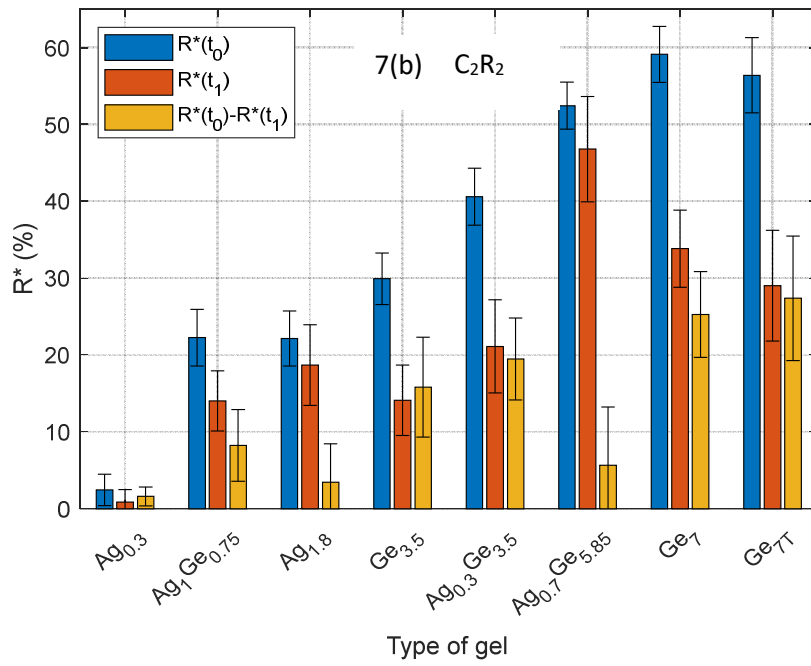
Figure 5

Figure 6

Figure 7

Figure 8
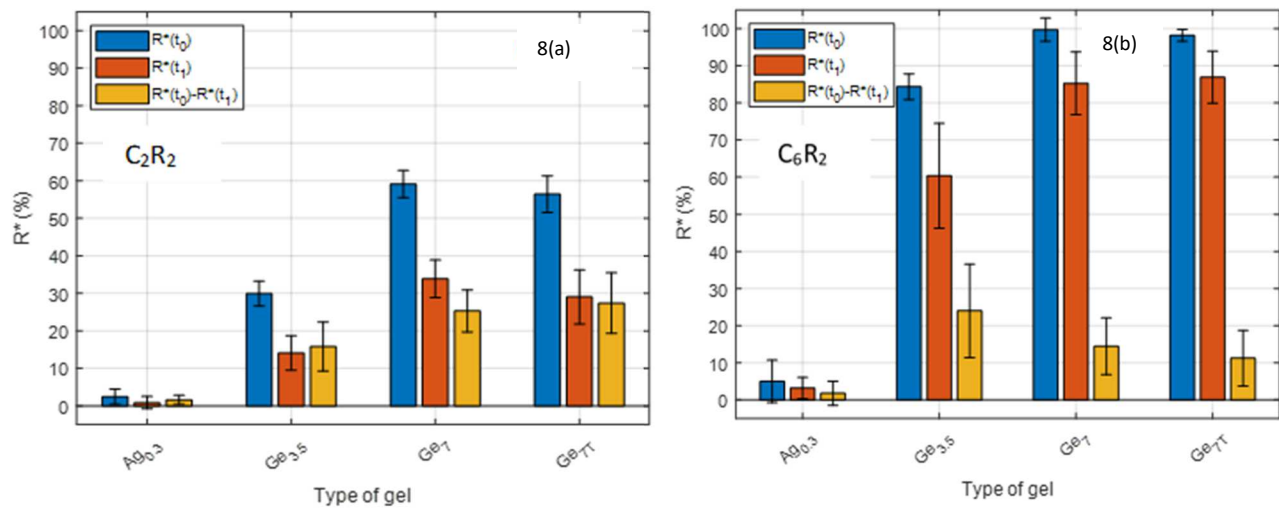
Figure 9

737
738
739
740
741
742
743
744
745
746
747
748
749
750
751
752
753
754
755
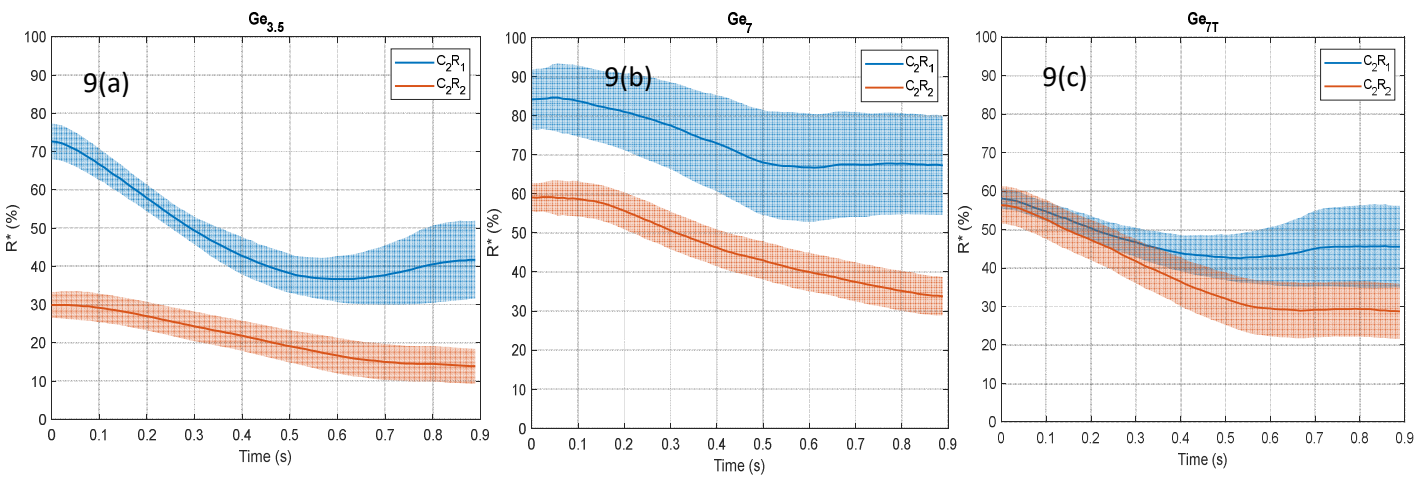
Table 1

Gel type	Composition (% wt)				Young's modulus (kPa)	Water released (g)
	Water	Agar	Gelatin	TWEEN 20		
$Ag_{0.3}$	84.7	0.3	-	-	4 ± 3	0.150 ± 0.020* (without compression)
$Ag_1Ge_{0.75}$	83.25	1	0.75	-	58 ± 15	0.257 ± 0.020
$Ag_{1.8}$	83.2	1.8	-	-	132 ± 10	0.151 ± 0.012
$Ge_{3.5}$	81.5	-	3.5	-	2 ± 0.1	0.028 ± 0.002
$Ag_{0.3}Ge_{3.5}$	81.2	0.3	3.5	-	13 ± 3	0.029 ± 0.004
$Ag_{0.7}Ge_{5.85}$	78.45	0.7	5.85	-	32 ± 7	0.015 ± 0.003
Ge_7	78	-	7	-	24 ± 2	0.015 ± 0.002
Ge_7T	76.5	-	7	1.5	17 ± 2	0.012 ± 0.001

766   Table 2

ATM type	No. of freezing/ thawing cycles	Young's modulus (kPa)	Surface profile (µm)		Water released (g)
			Peak height (R_a)	Correlation length (β)	
C_2R_1	2	23 ± 1	42 ± 1	289 ± 36	0.022 ± 0.002
C_2R_2	2	18 ± 1	72 ± 14	435 ± 62	0.031 ± 0.003
C_6R_1	6	71.2 ± 1	55 ± 3	341 ± 62	0.015 ± 0.002
C_6R_2	6	71 ± 2	103 ± 3	429 ± 63	0.018 ± 0.003

767

768

769

770

771

772

773

774

775

776

777